



**HAL**  
open science

# Mueller matrix polarimetry of bianisotropic materials [Invited]

Oriol Arteaga, Bart Kahr

► **To cite this version:**

Oriol Arteaga, Bart Kahr. Mueller matrix polarimetry of bianisotropic materials [Invited]. Journal of the Optical Society of America B, 2019, 10.1364/JOSAB.36.000F72 . hal-02437038

**HAL Id: hal-02437038**

**<https://polytechnique.hal.science/hal-02437038>**

Submitted on 16 Jan 2020

**HAL** is a multi-disciplinary open access archive for the deposit and dissemination of scientific research documents, whether they are published or not. The documents may come from teaching and research institutions in France or abroad, or from public or private research centers.

L'archive ouverte pluridisciplinaire **HAL**, est destinée au dépôt et à la diffusion de documents scientifiques de niveau recherche, publiés ou non, émanant des établissements d'enseignement et de recherche français ou étrangers, des laboratoires publics ou privés.



# Mueller matrix polarimetry of bianisotropic materials [Invited]

Oriol Arteaga, Bart Kahr

► **To cite this version:**

Oriol Arteaga, Bart Kahr. Mueller matrix polarimetry of bianisotropic materials [Invited]. Journal of the Optical Society of America B, Optical Society of America, 2019, 10.1364/JOSAB.36.000F72 . hal-02437038

**HAL Id: hal-02437038**

**<https://hal-polytechnique.archives-ouvertes.fr/hal-02437038>**

Submitted on 16 Jan 2020

**HAL** is a multi-disciplinary open access archive for the deposit and dissemination of scientific research documents, whether they are published or not. The documents may come from teaching and research institutions in France or abroad, or from public or private research centers.

L'archive ouverte pluridisciplinaire **HAL**, est destinée au dépôt et à la diffusion de documents scientifiques de niveau recherche, publiés ou non, émanant des établissements d'enseignement et de recherche français ou étrangers, des laboratoires publics ou privés.

# Mueller matrix polarimetry of bianisotropic materials

ORIOL ARTEAGA,<sup>1,2,4</sup> AND BART KAHR<sup>3,5</sup>

<sup>1</sup>*Dep. Física Aplicada, Feman Group, IN2UB, Universitat de Barcelona, Barcelona, Spain.*

<sup>2</sup>*LPICM, CNRS, École Polytechnique, IPParis, 91128 Palaiseau, France.*

<sup>3</sup>*Department of Chemistry and the Molecular Design Institute, New York University, New York, New York, USA*

<sup>4</sup>[oarteaga@ub.edu](mailto:oarteaga@ub.edu)

<sup>5</sup>[bart.kahr@nyu.edu](mailto:bart.kahr@nyu.edu)

**Abstract:** Mueller Matrix polarimetry is a powerful optical technique for the characterization of both anisotropic and bianisotropic materials. This review emphasizes methods for the interpretation of measured Mueller matrices, from the meanings of matrix symmetries, to *ab initio* calculations of Mueller matrices that begin with Maxwell's equations operating on materials with permittivity, permeability and magnetoelectric constitutive tensors. We present an overview of polarimetry measurements in crystals as well as metamaterials that have optically responsive features on the order of the wavelength of visible light. Examples of the full measurement of the constitutive tensors of bianisotropic media from the analysis of their Mueller matrix, collected either in transmission or reflection, are illustrated for natural crystals, polycrystals and nanofabricated metamaterials. Experimental and theoretical research into the complex optical responses of bianisotropic materials with polarized light is best expressed in terms of the Mueller matrix, as it offers an unambiguous and mathematically robust platform for analysis of light-matter interactions.

## 1. Introduction

Optical polarimetry can be used for the characterization of bianisotropic materials, those that have an orientational dependence with respect to the refraction of both linear and circularly polarized light. Arago's first polarimetric experiment revealed optical rotatory dispersion (*polarisation chromatique* in his words) [1, 2] from light, linearly polarized by reflection, passed along the high symmetry axis of  $\alpha$ -quartz, the first and most frequently studied bianisotropic material. By the middle of the 19th century, polarimetry was an established analytical technique for measuring the concentration of chiral analytes in a solution [3], i.e. a biisotropic medium. Polarimetry became essential to the characterization of natural products and to the determination of chemical reaction mechanisms [4].

Nineteenth century polarimetry was focused on perturbations to the state of linearly polarized light traversing a medium. Here, we emphasize Mueller matrix polarimetry in which many polarization states of light serve as modulated input, while the polarization of the output light is fully assayed. This more complete and complex form of polarimetry has the potential to provide a much fuller characterization of light-matter interactions. Mueller matrix polarimetry is derived from the development of the Stokes-Mueller optical calculus in the early part of the 20th century [5, 6].

The Mueller matrix represents the transfer function of an optical system in its interactions with polarized light and it contains all of the necessary information about the linear optical properties of the medium. The theory predated experiment, as few attempts to measure the complete Mueller matrix were made [7] until the availability of accurate electrophotometry and automated instruments capable of making intensity measurements with various independent combinations

of polarizers and retarders in the incoming and outgoing light beams [8, 9]. Nowadays Mueller matrix polarimetry is relatively well-acknowledged but, in general, it is still rarely applied if, for example, is compared with petrographic microscopes fitted with crossed linear polarizers, or simple polarization modulation schemes that compare of the transmission of alternating left and right circular polarization states, as in the case of circular dichroism spectrometers.

This paper is organized in three main sections that follow this introduction: Section 2 offers a basic introduction to the Stokes-Mueller formalism; Section 3 presents methods for the analysis of Mueller matrix polarimetric data of bianisotropic materials; Section 4 reviews experimental studies of bianisotropic materials using Mueller polarimetry. We have eschewed discussions about instrumental developments of spectroscopic and imaging Mueller polarimeters as they have been sufficiently described [10–13]. Nevertheless, further developments in instrumentation to increase sensitivity and spatial resolution will be required to ensure the vitality of Mueller matrix polarimetry in future.

## 2. Basic concepts

Any polarization state of light, either polarized, partially polarized or unpolarized can be represented by a Stokes vector  $\mathbf{S}$ . The Stokes vector has four real components that can be expressed in terms of intensities:  $S_0$  is the total intensity;  $S_1$  is the intensity difference in  $x$  and  $y$  polarizations;  $S_2$  is the difference between  $x'$  and  $y'$  vibrations, rotated by  $45^\circ$  with respect to  $xy$ ;  $S_3$  is the difference between left and right circular polarizations. These intensities can be transformed by a  $4 \times 4$  matrix with 16 real elements, the Mueller matrix  $\mathbf{M}$  [5, 14], which connects the input and output Stokes vectors after interaction of electromagnetic radiation with an optical medium by reflection, transmission, or scattering. However, not all real-valued  $4 \times 4$  matrices are Mueller matrices. Realizable Mueller matrices must connect physically realizable Stokes vectors. Almost the whole Stokes-Mueller formalism can be developed from this comparatively simple idea [15].

Mueller matrix polarimeters employ a polarization state generator (PSG) and a polarization state analyzer (PSA) to respectively produce and analyze polarization states as illustrated in Fig. 1. The PSG is in the path of the excitation beam probing the sample and the PSA is in the detection beam collected after interaction with the sample. Combining four (or more) input Stokes vectors generated by the PSG with four (or more) output vectors analyzed by the PSA results in a matrix of 16 measured (or more) light intensities that permit the determination of the 16 elements of the Mueller matrix of the sample. Mueller matrix polarimetry is described as complete polarimetry [11, 12], as opposed to partial polarimetry where only a subset of Mueller matrix elements are measured with simpler PSG and/or PSA devices and limitations on the polarization states that are generated and analyzed. Under special conditions it is possible to convert partial polarimetry measurements based on the determination of 9 or 12 Mueller matrix elements into complete Mueller matrices [16, 17]. Circular dichroism spectrometers are, for example, partial polarimeters optimized for measuring only one of the 16 elements of the Mueller matrix. Obtaining the remaining 15 elements, the complete Mueller matrix, is a formal prerequisite for the application of powerful algebraic decomposition methods that provide a phenomenological interpretation of complex media and systems in physical terms.

A non-depolarizing medium (material or system) that interacts linearly with a polarized light probe is generally described by a  $2 \times 2$  complex matrix  $\mathbf{J}$ , called the Jones matrix, transforming the incident transverse electric field vector into an outgoing vector following the interaction [18]. This Jones matrix will have a corresponding non-depolarizing Mueller matrix  $\mathbf{M}_{nd}$  with up to 7 independent parameters (the “absolute phase” of  $\mathbf{J}$  is not embodied in  $\mathbf{M}_{nd}$ ). If, furthermore, the medium under investigation is varying in space or in time (within the spatial or temporal resolution of the measurement equipment), then it cannot be described by a single Jones matrix, but rather by a statistical ensemble of Jones matrices or non-depolarizing Mueller matrices. This

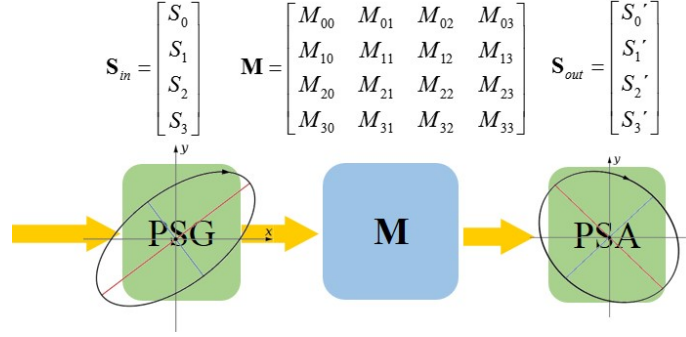


Fig. 1. Scheme of a PSG and PSA respectively probing a Mueller matrix and analyzing the resulting Stokes vector after the light-matter interaction.

statistical ensemble is formally equivalent to a Mueller matrix as it is schematically illustrated in Fig. 2. In this case,  $\mathbf{M}$  is called depolarizing, since it generally produces partially polarized outgoing light from totally polarized incident light.

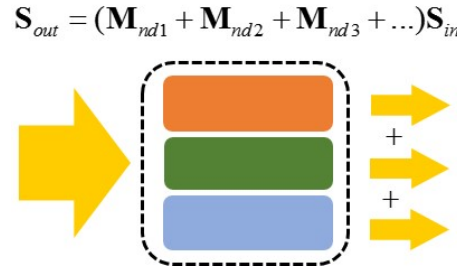


Fig. 2. Scheme of depolarizing system that can be understood as a statistical ensemble of parallel non-depolarizing contributions.

We can associate a coherency matrix  $\mathbf{C}$  with the Mueller matrix  $\mathbf{M}$  in the following way [15]:

$$\mathbf{C} = \frac{1}{4} \sum_{i,j=0}^3 M_{ij} \Pi_{ij}, \quad (1)$$

where  $M_{ij}(i, j = 0, 1, 2, 3)$  are the elements of the Mueller matrix  $\mathbf{M}$ ,  $\Pi_{ij} = \mathbf{A}(\sigma_i \otimes \sigma_j^*)\mathbf{A}^{-1}$ .

$$\mathbf{A} = \begin{pmatrix} 1 & 0 & 0 & 1 \\ 1 & 0 & 0 & -1 \\ 0 & 1 & 1 & 0 \\ 0 & i & -i & 0 \end{pmatrix}, \quad \mathbf{A}^{-1} = \frac{1}{2}\mathbf{A}^\dagger = \frac{1}{2} \begin{pmatrix} 1 & 1 & 0 & 0 \\ 0 & 0 & 1 & -i \\ 0 & 0 & 1 & i \\ 1 & -1 & 0 & 0 \end{pmatrix}. \quad (2)$$

The superscript  $\dagger$  indicates the conjugate transpose (Hermitian conjugate), the superscript  $*$  indicates the complex conjugate,  $\otimes$  is the Kronecker product and  $\sigma_i$  are the Pauli matrices with

the  $2 \times 2$  identity in the following order:

$$\sigma_0 = \begin{pmatrix} 1 & 0 \\ 0 & 1 \end{pmatrix}, \quad \sigma_1 = \begin{pmatrix} 1 & 0 \\ 0 & -1 \end{pmatrix}, \quad (3)$$

$$\sigma_2 = \begin{pmatrix} 0 & 1 \\ 1 & 0 \end{pmatrix}, \quad \sigma_3 = \begin{pmatrix} 0 & -i \\ i & 0 \end{pmatrix}. \quad (4)$$

If and only if the Mueller matrix of the system is non-depolarizing (alternatively *pure* or *deterministic*), the associated coherency matrix  $\mathbf{C}$  will be of rank one. When  $\text{rank}(\mathbf{C}) = 1$ , the single non-vanishing eigenvalue is  $\lambda_0 = \text{tr}(\mathbf{C}) = 1$ . In practice, due to the unavoidable noise, experimental Mueller matrices are never strictly non-depolarizing. A non-depolarizing estimate of a depolarizing Mueller matrix is found by constructing the Jones matrix from the eigenvector corresponding to the largest eigenvalue of  $\mathbf{C}$  [19]. If this eigenvector is  $(\tau \ \alpha \ \beta \ \gamma)^T$ , then the Jones matrix is [20]:

$$\mathbf{J} = \tau\sigma_0 + \alpha\sigma_1 + \beta\sigma_2 + \gamma\sigma_3 = \begin{pmatrix} \tau + \alpha & \beta - i\gamma \\ \beta + i\gamma & \tau - \alpha \end{pmatrix}. \quad (5)$$

and  $\mathbf{M}_{nd} = \mathbf{A}(\mathbf{J} \otimes \mathbf{J}^*)\mathbf{A}^{-1}$  is the Mueller matrix non-depolarizing estimate. Besides allowing to calculate this non-depolarizing estimate, coherency matrices are essential for a deeper mathematical understanding of Mueller matrices [21]. For example, they are useful to model situations of partial coherence [22, 23], to study depolarizing Mueller matrices from a statistical point of view [24] or to define a quaternion algebra for the Stokes-Mueller formalism [25].

A widely used method to quantify depolarization in experimental Mueller matrices is the depolarization index (DI) [26]:

$$\text{DI} = \frac{\sqrt{\sum_{i,j=0}^3 M_{ij}^2 - M_{00}^2}}{\sqrt{3}M_{00}}, \quad (6)$$

with values that vary between 0 for a perfect depolarizer to 1 for a non-depolarizing Mueller matrix. The DI may be sometimes used as a quality control index of a measurement system, especially when studying materials that we presume are of high quality and non-depolarizing.

### 2.1. Mueller matrix symmetries

The symmetries of Mueller matrices are insightful no matter the values of the elements themselves. In this section, we will focus our attention on the interpretation of symmetries for Mueller matrices measured at normal incidence in transmission or back reflection, i.e. for geometries where there is no preferential plane of scattering.

For normal incidence transmission measurements the most general symmetries that one can obtain for various media are summarized in Table 1. A more comprehensive list of Mueller matrix symmetries at random scattering angles is given in [27] and the symmetries that apply under specular reflection are discussed in [28]. The symmetries shown apply to depolarizing as well as non-depolarizing Mueller matrices. The symmetries of this table do not consider polarimetric reciprocity. Reversing the direction of light propagation in a medium that maintains polarimetric reciprocity should not change the experiment, i.e. the Stokes vector measured at the output must be the same after reversing the wave vector. We emphasize that *polarimetric reciprocity* is not equivalent to the more fundamental *electromagnetic reciprocity*, a concept that is important in the consideration of constitutive relations of bianisotropic materials [29].

**Table 1. Mueller matrix symmetries in normal incidence transmission**

Material	Symmetry description	Mueller matrix symmetry
Isotropic	Rotational symmetry and mirror symmetry	$\begin{pmatrix} M_{00} & 0 & 0 & 0 \\ 0 & M_{11} & 0 & 0 \\ 0 & 0 & M_{11} & 0 \\ 0 & 0 & 0 & M_{33} \end{pmatrix}$
Biisotropic	Rotational symmetry	$\begin{pmatrix} M_{00} & 0 & 0 & M_{03} \\ 0 & M_{11} & M_{12} & 0 \\ 0 & -M_{12} & M_{11} & 0 \\ M_{30} & 0 & 0 & M_{33} \end{pmatrix}$
Anisotropic	Mirror symmetry	$\begin{pmatrix} M_{00} & M_{01} & M_{02} & M_{03} \\ M_{01} & M_{11} & M_{12} & M_{13} \\ M_{02} & M_{12} & M_{22} & M_{23} \\ -M_{30} & -M_{13} & -M_{23} & M_{33} \end{pmatrix}$
Bianisotropic	No symmetry	$\begin{pmatrix} M_{00} & M_{01} & M_{02} & M_{03} \\ M_{10} & M_{11} & M_{12} & M_{13} \\ M_{20} & M_{21} & M_{22} & M_{23} \\ M_{30} & M_{31} & M_{32} & M_{33} \end{pmatrix}$

Unlike electromagnetic reciprocity, polarimetric reciprocity is easily broken even by ordinary anisotropic materials [30].

Table 2 summarizes symmetries when polarimetric reciprocity. The Table is split between normal incidence transmission and back reflection configurations. The back reflection case involves, by default, polarimetric reciprocity [31]. As such, this case is only considered in this table and not in Table 1.

### 3. Analysis of Mueller matrix polarimetry data

Raw polarimetric data can be analyzed at different levels: (1) The phenomenological optical properties of the sample, such as linear birefringence or linear dichroism, explain how the sample responds to polarized light quantitatively. This analysis alone is not necessarily informative about the sample's intrinsic dielectric, magnetic or magnetoelectric material tensors. (2) Alternatively, preliminary knowledge of the sample is used to construct an electromagnetic model that calculates, from material constituents, polarimetric results that are as close as possible to measurements. These two approaches will be presented in more detail in the next two subsections.

**Table 2. Mueller matrix symmetries with polarimetric reciprocity: normal incidence transmission and backreflection**

Material	Symmetry transmission	Symmetry backreflection
Isotropic	$\begin{pmatrix} M_{00} & 0 & 0 & 0 \\ 0 & M_{11} & 0 & 0 \\ 0 & 0 & M_{11} & 0 \\ 0 & 0 & 0 & M_{33} \end{pmatrix}$	$\begin{pmatrix} M_{00} & 0 & 0 & 0 \\ 0 & M_{11} & 0 & 0 \\ 0 & 0 & -M_{11} & 0 \\ 0 & 0 & 0 & M_{33} \end{pmatrix}$
Biisotropic	$\begin{pmatrix} M_{00} & 0 & 0 & M_{03} \\ 0 & M_{11} & M_{12} & 0 \\ 0 & -M_{12} & M_{11} & 0 \\ M_{03} & 0 & 0 & M_{33} \end{pmatrix}$	$\begin{pmatrix} M_{00} & 0 & 0 & M_{03} \\ 0 & M_{11} & 0 & 0 \\ 0 & 0 & -M_{11} & 0 \\ M_{03} & 0 & 0 & M_{33} \end{pmatrix}$
Anisotropic	$\begin{pmatrix} M_{00} & M_{01} & 0 & 0 \\ M_{01} & M_{11} & 0 & 0 \\ 0 & 0 & M_{22} & M_{23} \\ 0 & 0 & -M_{23} & M_{33} \end{pmatrix}$	$\begin{pmatrix} M_{00} & M_{01} & M_{02} & M_{03} \\ M_{01} & M_{11} & M_{12} & M_{13} \\ -M_{02} & -M_{12} & M_{22} & M_{23} \\ M_{03} & M_{13} & -M_{23} & M_{33} \end{pmatrix}$
Bianisotropic	$\begin{pmatrix} M_{00} & M_{01} & M_{02} & M_{03} \\ M_{01} & M_{11} & M_{12} & M_{13} \\ -M_{02} & -M_{12} & M_{22} & M_{23} \\ M_{03} & M_{13} & -M_{23} & M_{33} \end{pmatrix}$	$\begin{pmatrix} M_{00} & M_{01} & M_{02} & M_{03} \\ M_{01} & M_{11} & M_{12} & M_{13} \\ -M_{02} & -M_{12} & M_{22} & M_{23} \\ M_{03} & M_{13} & -M_{23} & M_{33} \end{pmatrix}$

### 3.1. Phenomenological calculation of optical properties

The two-by-two Jones matrix formalism for polarization optics can be defined in terms of eight real parameters (CD, LD, LD', CB, LB, LB',  $\eta$  and  $k$ ): [32, 33]:

$$\mathbf{J} = e^{-i\chi/2} \begin{pmatrix} \cos \frac{\Gamma}{2} - \frac{iL}{T} \sin \frac{\Gamma}{2} & \frac{(C-iL')}{T} \sin \frac{\Gamma}{2} \\ -\frac{(C+iL')}{T} \sin \frac{\Gamma}{2} & \cos \frac{\Gamma}{2} + \frac{iL}{T} \sin \frac{\Gamma}{2} \end{pmatrix}, \quad (7)$$

where

$$T = \sqrt{L^2 + L'^2 + C^2}, \quad (8)$$

$$\chi \equiv 2(\eta - ik),$$

$$L \equiv LB - iLD,$$

$$L' \equiv LB' - iLD',$$

$$C \equiv CB - iCD. \quad (9)$$

These eight parameters represent only one of the many alternative ways that one can choose to parameterize a complex 2x2 matrix. The advantage of this parameterization with respect to others is that in the case of *light transmitted through a homogeneous medium* the eight parameters have a clear physical interpretation as circular dichroism (CD), circular birefringence (CB),

horizontal linear dichroism (LD), 45° linear dichroism (LD'), horizontal linear birefringence (LB), 45° linear birefringence (LB'), isotropic retardation ( $\eta$ ) and isotropic amplitude absorption ( $k$ ). These optical effects are defined in Table 3.

A non-depolarizing Mueller matrix,  $\mathbf{M}_{nd}$ , can also be written in terms of these parameters, although it leads to a lengthy algebraic result [32]. It can be more conveniently written as a matrix exponential [34–36]:

$$\mathbf{M}_{nd} = e^{\mathbf{L}}, \quad \mathbf{L} = \begin{pmatrix} -\kappa & -LD & -LD' & CD \\ -LD & -\kappa & CB & LB' \\ -LD' & -CB & -\kappa & -LB \\ CD & -LB' & LB & -\kappa \end{pmatrix}. \quad (10)$$

Alternatively, this exponential result can be obtained from the differential analysis of a Mueller matrix, which is shown schematically in Fig. 3 and given by

$$\frac{d\mathbf{M}}{dz} = \mathbf{m}\mathbf{M}. \quad (11)$$

This equation introduces the differential matrix  $\mathbf{m}$  that relates the  $\mathbf{M}$  matrix of a homogeneous anisotropic medium to its spatial derivative along the direction of propagation of light ( $z$ ). Essentially, Eq. (10) is the solution of this differential equation when  $\mathbf{M}$  is non-depolarizing (then  $\mathbf{L} = \mathbf{m}d$ , where  $d$  is the total accumulated path length). If  $\mathbf{M}$  is depolarizing, Eq. (11) still holds [37] and a similar exponential solution may exist but then  $\mathbf{L}$  no longer maintains the simple form of Eq. (10).

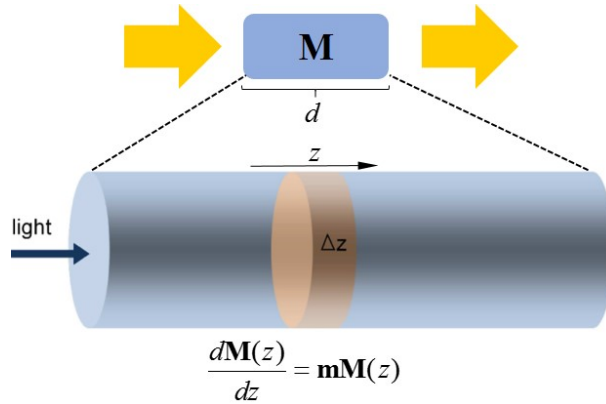


Fig. 3. Scheme of the differential analysis of a transmission Mueller matrix

We can conclude that, given an experimental transmission Mueller matrix, this differential analysis supports the calculation of interpretable optical properties merely by calculating the logarithm of the experimental matrix ( $\mathbf{L} = \ln\mathbf{M}$ ) or by analytically inverting Eq. (7) [33], after finding first a non-depolarizing estimate of the measured Mueller matrix as described in section 2. This type of analysis is often referred to as differential decomposition [38].

### 3.2. Comparison to a model

In most cases, if we want to obtain quantitative information about the values of the constitutive tensors of bianisotropic materials from Mueller matrix polarimetry, we must build a model that

**Table 3. Symbols used and definitions**

effect	symbol	definition <sup>a</sup>
isotropic phase retardation	$\eta$	$2\pi nl/\lambda_0$
isotropic amplitude absorption	$k$	$2\pi\kappa l/\lambda_0$
(x - y) linear dichroism	LD	$\frac{2\pi}{\lambda_0}(\kappa_x - \kappa_y)l$
(x - y) linear birefringence	LB	$\frac{2\pi}{\lambda_0}(n_x - n_y)l$
45° linear dichroism	LD'	$\frac{2\pi}{\lambda_0}(\kappa_{45} - \kappa_{135})l$
45° linear birefringence	LB'	$\frac{2\pi}{\lambda_0}(n_{45} - n_{135})l$
circular dichroism	CD	$\frac{2\pi}{\lambda_0}(\kappa_- - \kappa_+)l$
circular birefringence	CB	$\frac{2\pi}{\lambda_0}(n_- - n_+)l$

<sup>a</sup>  $n$  stands for refractive index,  $\kappa$  for the extinction coefficient,  $l$  for path length through the medium, and  $\lambda_0$  for the vacuum wavelength of light. Subscripts specify the polarization of light as,  $x$ ,  $y$ , 45° to the  $x$ -axis, 135° to the  $x$ -axis, circular right +, or left -.

establishes a link between constitutive tensors and Mueller or Jones matrices [39–43]. In other words, since experiment delivers a Mueller matrix, theory likewise should deliver a Mueller matrix so that the two can be compared and the constitutive elements can be refined in order to fit the experiment matrix. A favorable situation is light reflection/transmission by a layered bianisotropic medium. These conditions are often met for homogeneous bianisotropic systems such as certain crystals and also in other structurally bianisotropic systems such as helicoidal nanostructures [44–47] or liquid crystals [48]. A suitable matrix calculus was developed by Berreman [42] and it has the advantage that it “naturally” incorporates a bianisotropic set of constitutive relations [49, 50]. Modifications of this method to consider the partial coherence of light have also been developed [23, 51, 52]. We recently modified the matrix method by Yeh [43] for light propagation in layered anisotropic media so as to incorporate a bianisotropic form of the constitutive relations [53].

The constitutive equations that we consider in this work are:

$$\mathbf{D} = \boldsymbol{\varepsilon}\mathbf{E} + i\boldsymbol{\alpha}\mathbf{H}, \quad (12a)$$

$$\mathbf{B} = \boldsymbol{\mu}\mathbf{H} - i\boldsymbol{\alpha}^T\mathbf{E}, \quad (12b)$$

where  $\boldsymbol{\varepsilon}$ ,  $\boldsymbol{\mu}$  and  $\boldsymbol{\alpha}$  are, respectively, the permittivity, permeability and magnetoelectric (gyration) tensors (note that sometimes the magnetoelectric tensor is alternatively presented by the Greek letter  $\boldsymbol{\kappa}$ ). For a nonmagnetic material,  $\boldsymbol{\mu}$  is the identity 3×3 matrix tensor. For isotropic chiral media, a similar set of constitutive equations is used but  $\boldsymbol{\varepsilon}$ ,  $\boldsymbol{\mu}$  and  $\boldsymbol{\alpha}$  are scalars. We are unaware of any Mueller matrix measurement on a biisotropic media that is not chiral (thus requiring a more general set of constitutive equations). The Berreman [42] or Yeh [53] matrix methods can be used to model both the transmission and specular reflection of plane polarized light in layered bianisotropic media with these constitutive tensors. It is important to indicate that while both, transmission and reflection measurements, rely on the same set of bianisotropic relations, the way they probe the constitutive tensors is different [54]. Therefore, when studying bianisotropic materials, transmission and reflection measurements should be regarded as complementary (rather than alternative) approaches. Transmission measurements – only possible for transparent samples – are typically very sensitive to the anisotropy of the dielectric tensor  $\boldsymbol{\varepsilon}$  in the plane of

the sample, that manifests in differences between refractive indices, as anticipated in Table 3. In fact, at normal incidence, only the differences between refractive indices are probed, but not their “mean values”. The “mean values” are best studied for specular reflection measurements, a configuration that is referred to as ellipsometry. Conversely, for the magnetoelectric tensor  $\alpha$ , reflection measurements are insensitive to average values of this tensor, which are best studied in transmission. This will be illustrated for particular crystals in the next section.

Models for samples with large spatial dispersion effects such as in metamaterials with in-plane periodicity usually rely on numerical implementations of Maxwell equations as fields are propagated through discretized geometric models of materials that are being analyzed [55, 56]. Such simulations tend to be computer-intensive and often only achieve a qualitative agreement with measurements. Even so, some simple geometries allow for an analytic treatment, for example the case of a dipole dimer, which is important because it mimicks the situation commonly described as exciton coupling in organic chemistry [57]. This case can be studied with the coupled dipole method and it is possible to calculate and decompose the Mueller matrix for any scattering direction [58].

## 4. Experiments with bianisotropic materials

### 4.1. Crystals

Chiroptical measurements of single bianisotropic crystals along low symmetry directions has been a challenge for more than two centuries. While Arago observed the effects of optical rotatory dispersion when he passed linearly polarized light along the high symmetry axis of  $\alpha$ -quartz, it took 123 years before a credible measurement was made along the low symmetry diad axis using null polarimetry [59]. From 1983 onward, a systematic procedure for determining optical activity in low symmetry directions of bianisotropic crystals was developed by Kobayashi [60], Asahi [61] and coworkers using the generalized Jones matrix (Eq. 7) and a limited modulation scheme of a rotating polarizer and analyzer. However, typically this High Accuracy Universal Polarimetry (HAUP) employs normal incidence on plane parallel sections fashioned for each independent tensor element, albeit techniques have been introduced for correcting for the light path in oblique incidence [62, 63]. Mueller matrix polarimetry is an alternative whose merits are described in applications below.

As stated at the outset,  $\alpha$ -quartz has been the touchstone bianisotropic material that researchers have returned to time and again to validate new methods of polarimetry. The Mueller matrix of  $\alpha$ -quartz in transmission was first determined using a polarimeter with two photoelastic modulators whose orientations needed to be reconfigured so as to be able to solve the four linear equations that provide the 16 Mueller matrix elements [64]. Later, the magnetoelectric tensor of quartz was redetermined with four synchronously operating photoelastic modulators that did not require reconfiguration [65]. Obviating the mechanical movement of optical components is important for measuring comparatively small optical perturbations that arise in the magnetoelectric response of dissymmetric crystals. This sensitive four-photoelastic modulator polarimeter was also used to reinvestigate the linear electrogyration (electric field induced optical rotation) [66]. Even though it had been previously reported by others, this effect was no longer detectable with the new equipment. As this instrument permitted analytical separation of the independent polarimetric parameters, it avoided artifactual contributions from the large linear electro-optic effect, that most likely affected previous measurements.

Bianisotropic  $\text{AgGaS}_2$  was also reinvestigated [65] using the four-photoelastic modulator polarimeter [12]. This material was the focus of a milestone in the history of optical activity of bianisotropic substances. Hobden [67, 68] used a so-called isotropic point, an accidental isochrony in ordinary and extraordinary refractivities at one frequency, so as to measure CB in a low symmetry direction where the contribution from LB would ordinarily be withering. No such “tricks” are any longer required. Operating a Mueller matrix polarimeter in transmission

or reflection (a configuration usually known as Mueller matrix ellipsometry) gave independent determinations of the optical activity anisotropy of AgGaS<sub>2</sub> above the bandgap [69] without relying on accidental isochronies.

The number of anisotropic single crystals for which the magnetoelectric or gyration tensor has been determined completely is rather small given the >200 year history of the study of crystals with circularly polarized light (CPL). Those measured before the year 2000 were tabulated by Kaminsky [70] and those between 2000 and today by Martin [71]. The majority of these crystals were analyzed by HAUP but Mueller matrix polarimetry was recently used to analyze ethylene diammonium sulfate [72] and the isomorphous selenate [73]. These crystals, while isostructural, are distinct in that the selenate has an isotropic point at 364 nm (3.41 eV), where the ordinary and extraordinary refractive indices coincide. These subtle distinctions in optical response by experiment are necessary for challenging the computation of the refractivity of dielectric bianisotropic crystals, still a frontier in quantum chemistry requiring a linear response theory implemented with periodic boundary conditions. In other words, the anisotropy of the interaction of left and right CPL with single crystals remains a lingering aspect of linear crystal optics that is hard to define and are essential for understanding chiroptical structure-activity relationships.

Much of the literature on the optical properties of anisotropic media refer gyrotropy to the wave vector in the experiment. However, in the Berreman formulation discussed above, the magnetoelectric tensor must be defined, as for dielectric susceptibility, in terms of the orthogonal directions probed by the electric field vectors.

In the past, one of the most laborious steps in the analysis of the anisotropy of the optical activity of single crystal samples has been the necessity of obtaining polished, plane parallel slabs for each independent tensor element investigated. Some low symmetry molecular crystals resist cutting and polishing in the necessary directions. Benzil was a difficult organic crystal of this kind [74]. A tremendous savings in labor was achieved by accounting for multiply reflected incoherent waves in anisotropic, arbitrarily oriented crystals [75]. The Mueller matrix of thick crystals collected in transmission or reflection could then be interpreted in terms of the constitutive material parameters [22].

As a case study, we will review ethylene diammonium selenate [73]. Like its isomorphous sulfate, it is a lamellar crystal with a nearly perfect cleavage perpendicular to the optic axis. It is difficult to prepare plane polished sections in any other direction. Thin sections of several hundred micrometers were measured in transmission along the optic axis normal to the cleavage plane. The CB, twice the optical rotation, can be read straightaway, as the Mueller matrix in this configuration has the form of a rotation matrix and only depends on one parameter, the  $\alpha_{11}(\lambda)$  component of the magnetoelectric tensor. Reflection Mueller matrix data (Figure 4) were then acquired at several angles of incidence with respect to the optic axis, using the same crystal section as for the transmission data. Optical models for the crystal were then constructed using the techniques described in [22, 42, 75]. The  $\alpha_{33}(\lambda)$ ,  $\varepsilon_{11}(\lambda)$  and  $\varepsilon_{33}(\lambda)$  values were computed using standard dispersion equations with fitted parameters in order to achieve best fits with the spectroscopic Mueller matrix data. The orientation of the crystal and its thickness can also be refined as fitted values.

When plotted as in Figure 5a,  $\varepsilon_{11}$  and  $\varepsilon_{33}$  cross and, at this energy, LB drops to zero (Figure 5b). Where LB = 0, the crystal becomes accidentally optically isotropic and behaves as if it were an optically active, cubic crystal. This data can be displayed in several ways to emphasize the anisotropy of the optical activity as shown in Figure 5d-g. If the crystal section is mounted on a goniometer, polar maps of the CB can be displayed as a function of azimuthal orientation and tilt angle (Figure 5d-f). Alternatively, representation surfaces of the tensors can be plotted, either as  $\rho$  (deg/mm), or as the magnetoelectric parameter  $\alpha_{ij}$  (Figure 5g). The two presentations differ in that in one case, the anisotropy is projected onto a plane, whereas in the other the anisotropy is cast as a three-dimensional surface drawn with perspective on the paper. Because  $\rho$  (deg/mm) and

$\alpha_{ij}$  are bisignate, there are special directions on the surface of cones where the CB also vanishes and, at the isotropic point, light along these directions is wholly indifferent to polarization.

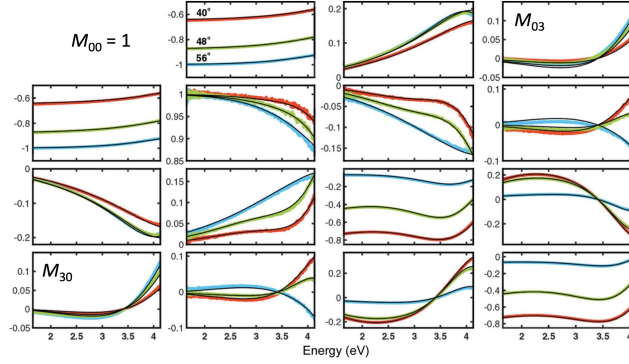


Fig. 4. Spectroscopic Mueller matrix for ethylene diammonium selenate, point group  $\bar{4}22$ , with a thickness of  $226 \mu\text{m}$  in reflection at three angles of incidence  $40^\circ$  (red),  $48^\circ$  (green),  $56^\circ$  (blue).

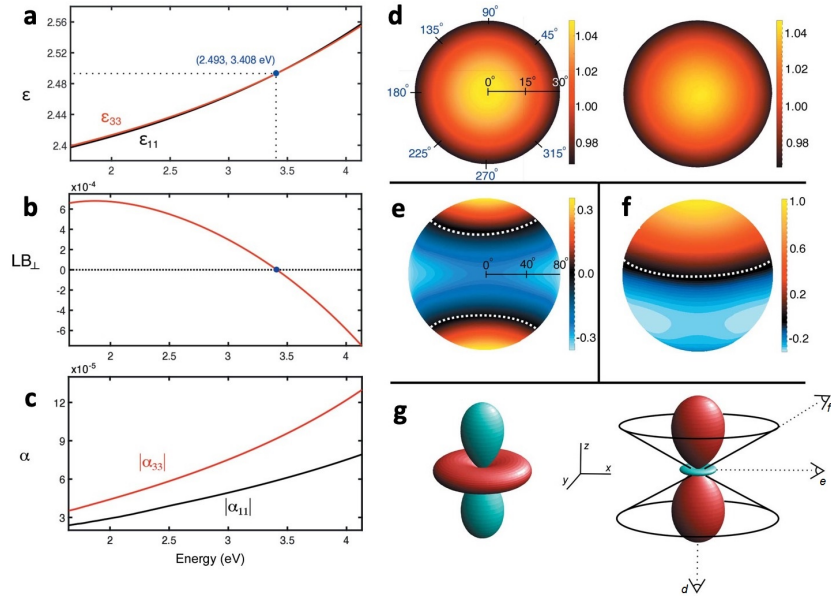


Fig. 5. The data in Figure 4 can be reduced to (a) the dielectric permittivity tensor components  $\epsilon$ , (b) the phenomenological linear birefringence (LB), and (c) the magnetolectric tensor elements components (d) experimental (left) and calculated (right) polar map of the circular birefringence at  $364 \text{ nm}$  ( $3.41 \text{ eV}$ ). Azimuthal and tilt angles are labeled. (e, f) Computed maps cut normal to  $[010]$  and  $63.9^\circ$  from  $[001]$ . (g) Normalized representation surfaces of the magnetolectric tensor  $\alpha$  (left) and of the optical rotation in  $\text{deg/mm}$  (right). The cones represent the places where both the linear birefringence and the circular birefringence disappear at one wavelength. The dashed lines indicate the viewing directions depicted in the polar maps in panels (d), (e) and (f), respectively.

The aforementioned Mueller matrix ellipsometry (reflection) of  $\text{AgGaS}_2$  measurements were

particularly instructive in focusing important distinctions between optical activity in transmission and optical activity in reflection, a subject investigated in the 1980's and 1990's by Silverman so as to evaluate competing sets of constitutive equations governing such phenomena. [69] Measurements of this kind have traditionally been challenging because unlike in transmission through transparent media, where optical activity accumulates over the optical path length of the material, reflection measurements sacrifice this enhancement. But, in the absorption band of a crystal like AgGaS<sub>2</sub>, resonance enhancement can make up for some of this difference. The complementarity between optically active, chiral ( $\alpha$ -quartz) and achiral (AgGaS<sub>2</sub>) uniaxial crystals is instructive and it is illustrated in Figure 6. Under normal incidence, the optical activity of  $\alpha$ -quartz cannot be measured. Silverman explained this by relying on the Ewald-Oseen extinction theorem, the idea that on reflection, opposite overlapping circular polarizations interfere [76]. However, it is easier to understand in this way: The ellipsometric parameters sensitive to optical activity record an azimuthal rotation of electric-field polarization as a transformation of *s*- and *p*-polarized inputs. However, in  $\alpha$ -quartz, under normal incidence along the optic axis, the electric field experiences equal components of the magnetoelectric tensor. Therefore, they both receive and transfer cross polarizations equivalently, and the response is given by the difference of these tensor elements, i.e. zero. On the other hand, in AgGaS<sub>2</sub>, the components of the magnetoelectric tensor normal to the optic axis are equal in magnitude but oppositely signed. In this symmetry, the reflection optical activity is equal to the difference between +/- values, and can indeed be measured.

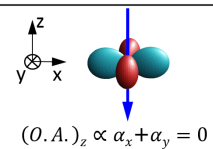
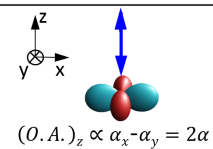
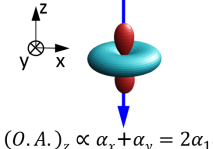
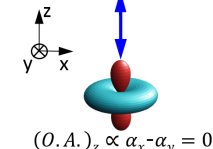
Point g.	Mag-elect. tensor	Transmission	Reflection
$\bar{4}2m$	$\begin{bmatrix} \alpha & 0 & 0 \\ 0 & -\alpha & 0 \\ 0 & 0 & 0 \end{bmatrix}$	 $(O.A.)_z \propto \alpha_x + \alpha_y = 0$	 $(O.A.)_z \propto \alpha_x - \alpha_y = 2\alpha$
32	$\begin{bmatrix} \alpha_{11} & 0 & 0 \\ 0 & \alpha_{11} & 0 \\ 0 & 0 & \alpha_{33} \end{bmatrix}$	 $(O.A.)_z \propto \alpha_x + \alpha_y = 2\alpha_{11}$	 $(O.A.)_z \propto \alpha_x - \alpha_y = 0$

Fig. 6. Transmission versus reflection optical activity for two optically active, uniaxial point groups 32 and  $\bar{4}2m$ . The dielectric tensor has the same form  $\epsilon = \text{diag}(\epsilon_{11}, \epsilon_{22}, \epsilon_{33})$ .  $(O.A.)_z$  means optical activity along the high-symmetry axis. Adapted from [69].

The response in a Mueller matrix polarimeter can be made vivid by exploring the wave vector space as in Fig. 7 where one point of the image corresponds to one direction of light propagation in the sample, producing a map of the *k*-vector distribution of the radiation. Such maps can be obtained in two different ways: using a high-NA objective and imaging its back focal plane with a technique that is named Mueller conoscopy [77, 78], the case is shown in Fig. 7, or using mechanical actuators to reorient the sample and/or the light beams to effectively scan the sample with a varying *k*-vector, a method used in Refs. [30, 79]. This representation is especially useful for exploring tensorial properties of materials. By accounting for the NA of the objective and the Euler angles that define the crystal orientation on the instrument, it is possible to use the previously discussed optical models to make simulations based on tensor constituents that are a best fit to the experimental data. The individual images can be read similar to the polar plots in Figure 5d-f although, in that case, the experimental data was not collected using a high-NA objective and a camera detector but reorienting the crystal in the Mueller matrix polarimeter and with a single point detector.

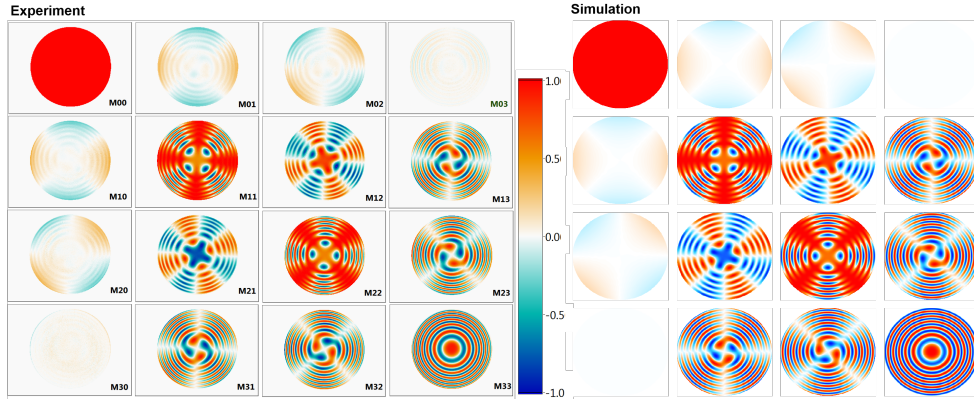


Fig. 7. Experiment and simulation of a 532 nm transmission Mueller matrix conoscopic measurement on a slab of  $z$ -cut (1 mm thick) right-handed  $\alpha$ -quartz. More details about these measurements in Ref. [78].

Recently, the optical activity anisotropy of potassium titanyl phosphate (KTP) has also been measured in reflection by Mueller matrix ellipsometry and the results have been analyzed according to different sets of constitutive equations [80]. As expected, only symmetric constitutive relations, such as those from Eq. (12), offer a satisfactory description of this reflection experiment. However, in transmission, only propagation of the electric field is needed to describe the linear optical activity. Adding an imaginary antisymmetric tensor to the permittivity tensor of the medium [53], as it is often described in classical books of optics or crystallography, can be adequate because these transmission experiments do not directly probe the change of the magnetic field. This is not the case for reflection experiments [69] that require bianisotropic constitutive equations to be properly described.

The synthesis of chiral zeolites or other micron-sized chiral particles has been a long-standing prize in catalysis. However, such crystallites tend to be difficult to study because they are too small for conventional polarimeters and sometimes they are ill-formed. Measurements are only possible with imaging methods that offer a high spatial resolution. Mueller matrix microscopy served to establish the absolute configuration of ellipsoidally-shaped enantiomorphs. The thinnest parts of the crystal were examined so that the order of the birefringence of samples remained first order, and so the circular birefringence could be evaluated as a signature of configuration straightaway [81].

#### 4.2. Metamaterials

Nanofabricated structures and metamaterials have made chiroptics a vital part of contemporary materials science [82]. Applications of strong responses range from negative index substances, [83] to broadband circular polarizers [84] and optical chirality enhancers [85].

The metamaterials analyzed here are regularly arrayed nanostructured composites. When the lattice constant of the array is small as compared to the wavelength, the optical response of the material can be described by effective properties. The nanostructures are engineered so as to establish the permittivity and permeability *a priori*, often relying on large optical activity as a consequence of amplified spatial dispersion with respect to the wavelength of light. The wavelength to lattice constant ratio above which effective optical constants can be attributed to the metamaterial is a matter of debate.

Various periodic arrays of split-ring resonators have been studied by Mueller matrix polarimetry [56, 79, 86–88] at oblique incidence in the visible and IR spectral range. Even if metamaterials are

fabricated on a planar substrate, bianisotropy in terms of magnetoelectric coupling manifests at oblique incidence whenever the plane of incidence is not coinciding a mirror-plane of the sample. A similar response was found for oblique arrays of perforated holes in gold [30]. At normal incidence, however, magnetoelectric coupling effects cannot be excited for strictly planar systems, albeit it is still possible to have phenomena such as asymmetric transmission of CPL [30, 89]. This is shown in Fig. 8a for the oblique array of holes in gold measured at normal incidence. Note that the two directions of propagation considered (forward and backward) carry the same amount of CPL (Fig. 8b) thus showing the reciprocal response of the medium. For reciprocal media we can state that *if two incident beams of equal intensity and equal polarization but opposite direction emerge from a medium, the same polarization components of the light must have equal intensities*.

In principle, ideal planar metamaterials should be described as anisotropic materials instead of bianisotropic because they are achiral. Fabricated metamaterials, even if designed to be thin "two-dimensional" structures, are in reality quasi-planar if they lie on a substrate; they become dissymmetric by virtue of the backing to which they are affixed. Moreover, oftentimes, electron beam lithography can lead to unintended rounding of the edges of nanostructures on the exposed side, heightening this dissymmetry. This can generate a significant bianisotropic response even at normal incidence [90].

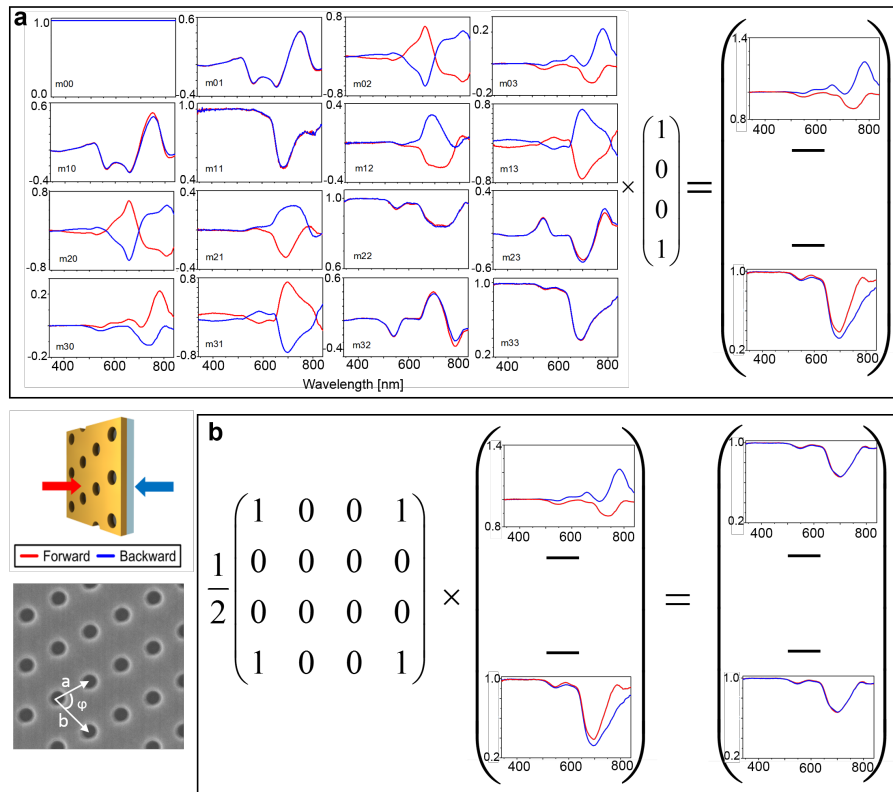


Fig. 8. Spectroscopic Mueller matrix measurement of the oblique array lattice of holes in a gold film in the forward and backward configurations. The diameter of the holes is 250 nm and the lattice parameters are  $a = 530$  nm,  $b = 730$  nm and  $\phi = 65^\circ$ . **a** shows that forward and backward measurements lead to a different overall transmitted intensity. **b** shows that if the resulting Stokes vector is analyzed by a circular polarizer, the transmitted intensity will be the same in both configurations. Adapted from [30].

Thin film metamaterials also have been intensively studied by Mueller matrix ellipsometry, particularly in the case of chiral sculpted thin films [46, 47, 91, 92] that achieve selective reflection of circularly polarized light through circular Bragg resonances. This form-induced bianisotropy, in many ways analogous to the cholesteric phase of liquid crystals [93] and other supramolecular assemblies [94], or to the Bouligand structures of the cuticle of some beetles [44, 95], presents subtle differences in the optical manifestations compared to bianisotropic crystals, for example displaying differential reflection of CPL at normal incidence (backreflection). This is not possible upon reflection in biisotropic or bianisotropic crystals [54]. These differences stem from the constitutive equations themselves, since helical structures are described by the dielectric tensor of a homogeneous medium with a twist, without including a magnetoelectric response. Thus, they cannot be strictly considered bianisotropic. Nevertheless, there is still some relation between both concepts; only the length scale differs. For example, if the periodicity of the rotation in a helical medium, i.e. the helix pitch, is very small compared to the wavelength, the medium could be considered homogeneous and it could be described by the constitutive equations of bianisotropic media in Eq. 12.

Similarly, in certain polycrystalline samples, Mueller matrix polarimetry can give signatures of CB or CD that are not necessarily consequences of the complex magnetoelectric tensor, but rather arise from some degree of helical ordering. In fact, Mueller matrix polarimetry is especially sensitive to false chiroptical responses of this kind that arise in inhomogeneities in the propagation direction for which decompositions of Mueller matrices to their differential analogs are not appropriate. Nevertheless, the resulting artifactual signals of CB and CD can be very instructive for establishing mesoscale ordering of anisotropic components on the micron-scale, especially since such effects are only electric dipole allowed [96–103].

## 5. Conclusion

Complexity has placed bianisotropic optical materials at the forefront of contemporary experimental and theoretical studies. The common feature of these materials is that their properties cannot be correctly represented only with a permittivity tensor and the magnetoelectric tensors must be considered simultaneously. Mueller matrix polarimetry is the most general technique for analyzing the linear optical response to polarized light, thus it is specially suited to samples that exhibit anisotropy in the dielectric *and* magnetoelectric tensor.

For a given experimental Mueller matrix, even one with evident symmetries, it is not obvious whether it arises from a bianisotropic, anisotropic or even isotropic sample. The precious additional knowledge available to the experimentalist is the orientation of the sample with respect to the excitation and detection light beams. When this is known, it is possible to correlate the symmetry of the Mueller matrix with material symmetries that appear in the constitutive tensors. In such cases, for example, the anisotropy of the differential refraction and absorption of circularly polarized light completes the characterizations of linear light-matter interactions, quantities that have resisted interpretation for generations.

Mueller matrices of metamaterials and polycrystalline structures can often have large values associated with the dispersion or dissipation of circularly polarized light, whether they originate in natural optical activity or heterogeneities of complex anisotropic components. Chiroptical properties typically arise in the dissymmetric arrangement of polarizable atoms or groups of atoms. On the mesoscale, the differential Mueller matrix associated to transmission measurements provides evidence of the dissymmetric arrangement of misoriented anisotropic elements, polarimetric remnants of inhomogeneities along the light propagation direction, that can reveal details of structures within complex, organized media.

## Funding

Ministerio de Economía y Competitividad (MINECO) (CTQ2017-87864-C2-1-P and EUIN2017-88598) and European Commission (Polarsense, MSCA-IF-2017-793774). US National Science Foundation, DMR1105000 and DMR-1608374.

## Acknowledgments

BK is grateful to a number of doctoral students whose research has contributed to the content herein: J. Freudenthal, X. Cui, S. M. Nichols, A. Martin, and M. Tan.

## Disclosures

The authors declare that there are no conflicts of interest related to this article.

## References

1. D. F. Arago, "Sur une modification remarquable qu'éprouvent les rayons lumineux dans leur passage à travers certains corps diaphanes, et sur quelques autres nouveaux phénomènes d'optique," *Mem. Inst.* **1**, 93–134 (1811).
2. B. Kahr and O. Arteaga, "Arago's Best Paper," *ChemPhysChem* **13**, 79–88 (2012).
3. H. Landolt, D. C. Robb, and V. H. Veley, *Handbook of the Polariscope* (MacMillan and Co., 1882).
4. T. M. Lowry, *Optical Rotatory Power* (Longmans, Green and Company, 1935).
5. P. Soleillet, "Sur les paramètres caractérisant la polarisation partielle de la lumière dans les phénomènes de fluorescence," *Annales de Physique* **12**, 23–59 (1929).
6. K. Järrendahl and B. Kahr, "Hans Mueller (1900-1965)," (2011).
7. B. S. Pritchard and W. G. Elliott, "Two instruments for atmospheric optics measurements\*," *J. Opt. Soc. Am.* **50**, 191–202 (1960).
8. P. S. Hauge, "Mueller matrix ellipsometry with imperfect compensators," *J. Opt. Soc. Am.* **68**, 1519–1528 (1978).
9. R. M. A. Azzam, "Photopolarimetric measurement of the Mueller matrix by Fourier analysis of a single detected signal," *Opt. Lett.* **2**, 148–150 (1978).
10. R. M. A. Azzam, "Stokes-vector and Mueller-matrix polarimetry," *J. Opt. Soc. Am. A* **33**, 1396–1408 (2016).
11. R. A. Chipman, *Polarimetry in Handbook of Optics, Vol. II, Bass ed.* (McGraw-Hill, 1995).
12. O. Arteaga, J. Freudenthal, B. Wang, and B. Kahr, "Mueller matrix polarimetry with four photoelastic modulators: theory and calibration," *Appl. Opt.* **51**, 6805–6817 (2012).
13. O. Arteaga, M. Baldrís, J. Antó, A. Canillas, E. Pascual, and E. Bertran, "Mueller matrix microscope with a dual continuous rotating compensator setup and digital demodulation," *Appl. Opt.* **53**, 2236–2245 (2014).
14. F. Perrin, "Polarization of light scattered by isotropic opalescent media," *J. Chem. Phys.* **10**, 415–427 (1942).
15. J. J. Gil Pérez and R. Ossikovski, *Polarized Light and the Mueller Matrix Approach* (CRC Press, Taylor & Francis Group, 2016).
16. R. Ossikovski and O. Arteaga, "Complete mueller matrix from a partial polarimetry experiment: the nine-element case," *J. Opt. Soc. Am. A* **36**, 403–415 (2019).
17. O. Arteaga and R. Ossikovski, "Complete mueller matrix from a partial polarimetry experiment: the 12-element case," *J. Opt. Soc. Am. A* **36**, 416–427 (2019).
18. C. R. Jones, "New calculus for the treatment of optical systems. VII. Properties of the N-matrices," *J. Opt. Soc. Am.* **38**, 671–685 (1948).
19. S. R. Cloude, "Group theory and polarisation algebra," *Optik* **75**, 26–36 (1986).
20. E. Kuntman, M. Ali Kuntman, and O. Arteaga, "Vector and matrix states for Mueller matrices of nondepolarizing optical media," *J. Opt. Soc. Am. A* **34**, 80+ (2016).
21. J. J. Gil, "Polarimetric characterization of light and media: Physical quantities involved in polarimetric phenomena," *The Eur. Phys. J. - Appl. Phys.* **40**, 1â€47 (2007).
22. S. M. Nichols, O. Arteaga, A. Martin, and B. Kahr, "Transmission and reflection of light from a thick anisotropic crystal measured with a four photoelastic modulator polarimeter and modeled by an incoherent sum of partial waves," *J. Opt. Soc. Am.* **32**, 2049–2057 (2015).
23. S. Nichols, "Coherence in polarimetry," Ph.D. thesis, New York University (2018).
24. R. Ossikovski and O. Arteaga, "Statistical meaning of the differential mueller matrix of depolarizing homogeneous media," *Opt. Lett.* **39**, 4470–4473 (2014).
25. E. Kuntman, M. A. Kuntman, A. Canillas, and O. Arteaga, "Quaternion algebra for stokes&#x2013;mueller formalism," *J. Opt. Soc. Am. A* **36**, 492–497 (2019).
26. J. J. Gil and E. Bernabeu, "A depolarization criterion in Mueller matrices," *J. Mod. Opt.* pp. 259–261 (1985).
27. H. C. van de Hulst, *Light Scattering by Small Particles* (Dover Publications Inc., 1982).
28. O. Arteaga, "Useful Mueller matrix symmetries for ellipsometry," *Thin Solid Films* **571**, 584–588 (2014).
29. T. G. Mackay and A. Lakhtakia, "Electromagnetic fields in linear bianisotropic mediums," *Prog. Opt.* **51**, 121–209 (2008).

30. O. Arteaga, B. M. Maoz, S. Nichols, G. Markovich, and B. Kahr, "Complete polarimetry on the asymmetric transmission through subwavelength hole arrays," *Opt. Express* **22**, 13719–13732 (2014).
31. O. Arteaga, E. Garcia-Caurel, and R. Ossikovski, "Elementary polarization properties in the backscattering configuration," *Opt. Lett.* **39**, 6050–6053 (2014).
32. O. Arteaga, "Mueller matrix polarimetry of anisotropic chiral media," Ph.D. thesis, University of Barcelona (2010).
33. O. Arteaga and A. Canillas, "Analytic inversion of the Mueller-Jones polarization matrices for homogeneous media," *Opt. Lett.* **35**, 559–561 (2010).
34. J. Schellman and H. P. Jensen, "Optical spectroscopy of oriented molecules," *Chem. Rev.* **87**, 1359–1399 (1987).
35. O. Arteaga and B. Kahr, "Characterization of homogenous depolarizing media based on Mueller matrix differential decomposition," *Opt. Lett.* **38**, 1134–1136 (2013).
36. O. Arteaga, "Number of independent parameters in the Mueller matrix representation of homogeneous depolarizing media," *Opt. Lett.* **38**, 1131–1133 (2013).
37. R. Ossikovski, "Differential matrix formalism for depolarizing anisotropic media," *Opt. letters* **36**, 2330–2332 (2011).
38. O. Arteaga, "Historical revision of the differential Stokes-Mueller formalism: discussion," *J. Opt. Soc. Am. A* **34**, 410–414 (2017).
39. P. D. Rogers, T. D. Kang, T. Zhou, M. Kotelyanskii, and A. A. Sirenko, "Mueller matrices for anisotropic metamaterials generated using 4x4 matrix formalism," *Thin Solid Films* **519**, 2668–2673 (2011).
40. M. Schubert, T. E. Tiwald, and J. A. Woollam, "Explicit solutions for the optical properties of arbitrary magneto-optic materials in generalized ellipsometry," *Appl. Opt.* **38**, 177–187 (1999).
41. M. Schubert, "Generalized ellipsometry and complex optical systems," *Thin Solid Films* **313-314**, 323 – 332 (1998).
42. D. W. Berreman, "Optics in stratified and anisotropic media: 4x4-Matrix formulation," *J. Opt. Soc. Am.* **62**, 502–510 (1972).
43. P. Yeh, "Electromagnetic propagation in birefringent layered media," *J. Opt. Soc. Am.* **69**, 742–756 (1979).
44. H. Arwin, R. Magnusson, J. Landin, and K. Järrendahl, "Chirality-induced polarization effects in the cuticle of scarab beetles: 100 years after Michelson," *Philos. Mag.* **92**, 1583–1599 (2012).
45. H. Arwin, A. Mendoza-Galván, R. Magnusson, A. Andersson, J. Landin, K. Järrendahl, E. Garcia-Caurel, and R. Ossikovski, "Structural circular birefringence and dichroism quantified by differential decomposition of spectroscopic transmission Mueller matrices from *Cetonia aurata*," *Opt. Lett.* **41**, 3293–3297 (2016).
46. A. C. van Popta, J. C. Sit, and M. J. Brett, "Optical properties of porous helical thin films," *Appl. Opt.* **43**, 3632–3639 (2004).
47. N. J. Podraza, S. M. Pursel, C. Chen, M. W. Horn, and R. W. Collins, "Analysis of the optical properties and structure of serial bi-deposited TiO<sub>2</sub> chiral sculptured thin films using Mueller matrix ellipsometry," *J. Nanophotonics* **2**, 021930+ (2008).
48. D. Coursault, B. H. Ibrahim, L. Pelliser, B. Zappone, A. de Martino, E. Lacaze, and B. Gallas, "Modeling the optical properties of self-organized arrays of liquid crystal defects," *Opt. Express* **22**, 23182+ (2014).
49. T. N. Stanislavchuk, T. D. Kang, P. D. Rogers, E. C. Standard, R. Basistyy, A. M. Kotelyanskii, G. Nita, T. Zhou, G. L. Carr, M. Kotelyanskii, and A. A. Sirenko, "Synchrotron radiation-based far-infrared spectroscopic ellipsometer with full Mueller-matrix capability," *Rev. Sci. Instruments* **84**, 023901+ (2013).
50. T. Brakstad, M. Kildemo, Z. Ghadyani, and I. Simonsen, "Dispersion of polarization coupling, localized and collective plasmon modes in a metallic photonic crystal mapped by Mueller matrix ellipsometry," *Opt. Express* **23**, 22800+ (2015).
51. S. M. Nichols, O. Arteaga, A. T. Martin, and B. Kahr, "Partially coherent light propagation in stratified media containing an optically thick anisotropic layer," *Appl. Surf. Sci.* **421, Part B**, 571–577 (2016).
52. A. T. Martin, S. M. Nichols, M. Tan, and B. Kahr, "Mueller matrix modeling of thick anisotropic crystals with metallic coatings," *Appl. Surf. Sci.* **421**, 578–584 (2017).
53. R. Ossikovski and O. Arteaga, "Extended Yeh's method for optically active anisotropic layered media," *Opt. Lett.* **42**, 3690+ (2017).
54. O. Arteaga, "Natural optical activity vs circular bragg reflection studied by mueller matrix ellipsometry," *Thin Solid Films* **617**, 14–19 (2016).
55. W. Yin, "Scattering by a linear array of uniaxial bianisotropic chiral cylinders," *Microw. Opt. Technol. Lett.* **12**, 287–295.
56. N. Guth, S. Varault, J. Grand, G. Guida, N. Bonod, B. Gallas, and J. Rivory, "Importance of Mueller matrix characterization of bianisotropic metamaterials," *Thin Solid Films* **571**, 405–409 (2014).
57. B. Auguie, J. L. Alonso-Gómez, A. Guerrero-Martínez, and L. M. Liz-Marzán, "Fingers crossed: Optical activity of a chiral dimer of plasmonic nanorods," *The J. Phys. Chem. Lett.* **2**, 846–851 (2011). PMID: 26295617.
58. M. A. Kuntman, E. Kuntman, J. Sancho-Parramon, and O. Arteaga, "Light scattering by coupled oriented dipoles: Decomposition of the scattering matrix," *Phys. Rev. B* **98**, 045410 (2018).
59. G. Szivessy and C. Münster, "Über die Prüfung der Gitteroptik bei aktiven Kristallen," *Annalen der Physik* **20**, 703–736 (1934).
60. J. Kobayashi and Y. Uesu, "A new optical method and apparatus 'HAUP' for measuring simultaneously optical activity and birefringence of crystals. I. Principles and construction," *J. Appl. Crystallogr.* **16**, 204–211 (1983).
61. T. Asahi and J. Kobayashi, *Polarimeter for anisotropic optically active materials in Introduction to Complex Mediums for Optics and Electrodynamics* (SPIE Press, 2003).

62. W. Kaminsky and A. M. Glazer, "Measurement of optical rotation in crystals," *Ferroelectric* **183**, 133–141 (1996).
63. K. Claborn, J. Herreros Cedres, C. Isborn, A. Zozulya, E. Weckert, W. Kaminsky, and B. Kahr, "Optical rotation of achiral pentaerythritol," *Ferroelectric* **128**, 14746–14747 (2006).
64. O. Arteaga, A. Canillas, and J. Jellison, "Determination of the components of the gyration tensor of quartz by oblique incidence transmission two-modulator generalized ellipsometry," *Appl. Opt.* **48**, 5307–5317 (2009).
65. O. Arteaga, J. Freudenthal, B. Kahr, and IUCr, "Reckoning electromagnetic principles with polarimetric measurements of anisotropic optically active crystals," *J. Appl. Crystallogr.* **45**, 279–291 (2012).
66. A. Sen Gupta, O. Arteaga, R. Haislmaier, B. Kahr, and G. Venkataraman, "Reinvestigation of electric field-induced optical activity in  $\alpha$ -quartz: Application of a polarimeter with four photoelastic modulators," *Chirality* **26**, 430–433 (2014).
67. M. V. Hobden, "Optical activity in a non-enantiomorphous crystal silver gallium sulphide," *Nature* **216**, 678 (1967).
68. M. V. Hobden, "Optical activity in a non-enantiomorphous crystal: AgGaS<sub>2</sub>," *Acta Crystallogr.* **A24**, 676–680 (1968).
69. O. Arteaga, "Spectroscopic sensing of reflection optical activity in achiral AgGaS<sub>2</sub>," *Opt. Lett.* **40**, 4277–4280 (2015).
70. W. Kaminsky, "Experimental and phenomenological aspects of circular birefringence and related properties in transparent crystals," *Rep. Prog. Phys.* **63**, 1575 (2000).
71. A. T. Martin, "Optical Activity Anisotropy in Solids," Ph.D. thesis, New York University (2018).
72. S. Nichols, A. Martin, J. Choi, and B. Kahr, "Gyration and permittivity of ethylenediammonium sulfate crystals," *Chirality* **28**, 460–465 (2016).
73. A. T. Martin, M. Tan, S. M. Nichols, E. Timothy, and B. Kahr, "Revisiting polarimetry near the isotropic point of an optically active, non-enantiomorphous, molecular crystal," *Chirality* **30**, 841–849 (2018).
74. K. Nakagawa, A. T. Martin, S. M. Nichols, V. L. Murphy, B. Kahr, and T. Asahi, "Optical activity anisotropy of benzil," *J. Phys. Chem. C* **121**, 25494–25502 (2017).
75. K. Postava, T. Yamaguchi, and R. Kantor, "Matrix description of coherent and incoherent light reflection and transmission by anisotropic multilayer structures," *Appl. Opt.* **41**, 2521–2531 (2002).
76. M. Silverman, *Waves and Grains: Reflections on Light and Learning* (Princeton University Press, 1998).
77. J. Freudenthal, "Mueller matrix imaging in crystallography: The chiroptics of pattern formation," Ph.D. thesis, New York University (2011).
78. O. Arteaga, S. M. Nichols, and J. Anto, "Back-focal plane mueller matrix microscopy: Mueller conoscopy and mueller diffractometry," *Appl. Surf. Sci.* **421**, 702 – 706 (2017).
79. B. Gompf, B. Krausz, B. Frank, and M. Dressel, "k-dependent optics of nanostructures: Spatial dispersion of metallic nanorings and split-ring resonators," *Phys. Rev. B* **86**, 075462+ (2012).
80. C. Sturm, V. Zviagin, and M. Grundmann, "Applicability of the constitutive equations for the determination of the material properties of optically active materials," *Opt. Lett.* **617**, 14–19 (2019).
81. A. Rojas, O. Arteaga, B. Kahr, and M. A. Cambor, "Synthesis, structure, and optical activity of HPM-1, a pure silica chiral zeolite," *J. Am. Chem. Soc.* **135**, 11975–11984 (2013).
82. Z. Wang, F. Cheng, T. Winsor, and Y. Liu, "Optical chiral metamaterials: A review of the fundamentals, fabrication methods, and applications," *Nanotechnology* **27**, 412001 (2016).
83. J. B. Pendry, "A chiral route to negative refraction," *Science* **306**, 1353–1355 (2004).
84. J. K. Gansel, M. Thiel, M. S. Rill, M. Decker, K. Bade, V. Saile, G. von Freymann, S. Linden, and M. Wegner, "Gold helix photonic metamaterial as broadband circular polarizer," *Science* **325**, 1513–1515 (2009).
85. M. Schäferling, D. Dregely, M. Hentschel, and H. Giessen, "Tailoring enhanced optical chirality: Design principles for chiral plasmonic nanostructures," *Phys. Rev. X* **2**, 031010 (2012).
86. T. W. H. Oates, T. Shaykhtudinov, T. Wagner, A. Furchner, and K. Hinrichs, "Mid-infrared gyrotropy in split-ring resonators measured by Mueller matrix ellipsometry," *Opt. Mater. Express* **4**, 2646–2655 (2014).
87. T. W. H. Oates, B. Dastmalchi, C. Helgert, L. Reissmann, U. Huebner, E.-B. Kley, M. A. Verschuuren, I. Bergmair, T. Pertsch, K. Hingerl, and K. Hinrichs, "Optical activity in sub-wavelength metallic grids and fishnet metamaterials in the conical mount," *Opt. Mater. Express* **3**, 439+ (2013).
88. N. Guth, B. Gallas, J. Rivory, J. Grand, A. Ourir, G. Guida, R. Abdeddaim, C. Jouvaud, and J. de Rosny, "Optical properties of metamaterials: Influence of electric multipoles, magnetoelectric coupling, and spatial dispersion," *Phys. Rev. B* **85** (2012).
89. J. C. Wilson, P. Gutsche, S. Herrmann, S. Burger, and K. M. McPeak, "Correlation of circular differential optical absorption with geometric chirality in plasmonic meta-atoms," *Opt. Express* **27**, 5097–5115 (2019).
90. O. Arteaga, J. Sancho-Parramon, S. Nichols, B. M. Maoz, A. Canillas, S. Bosch, G. Markovich, and B. Kahr, "Relation between 2D/3D chirality and the appearance of chiroptical effects in real nanostructures," *Opt. Express* **24**, 2242+ (2016).
91. D. Schmidt, E. Schubert, and M. Schubert, "Generalized ellipsometry determination of non-reciprocity in chiral silicon sculptured thin films," *Phys. Status Solidi (A)* **205**, 748–751 (2008).
92. M. Oliva-Ramírez, V. J. Rico, J. Gil-Rostra, O. Arteaga, E. Bertran, R. Serna, A. R. González-Elipe, and F. Yubero, "Liquid switchable radial polarization converters made of sculptured thin films," *Appl. Surf. Sci.* **475**, 230 – 236 (2019).
93. M. Mitov, "Cholesteric liquid crystals with a broad light reflection band," *Adv. Mater.* **24**, 6260–6276.
94. A. Thomas, T. Chervy, S. Azzini, M. Li, J. George, C. Genet, and T. W. Ebbesen, "Mueller polarimetry of chiral

- supramolecular assembly," *J. Phys. Chem. C* **122**, 14205–14212 (2018).
95. R. Magnusson, C.-L. Hsiao, J. Birch, H. Arwin, and K. Järrendahl, "Chiral nanostructures producing near circular polarization," *Opt. Mater. Express* **4**, 1389+ (2014).
  96. J. Freudenthal, E. Hollis, and B. Kahr, "Imaging chiroptical artifacts," *Chirality* **21**, E20–E27 (2009).
  97. J. Freudenthal and B. Kahr, "Dendritic growth, asymmetric photochemistry, and the origin of biomolecular homochirality," *Chirality* **20**, 973–977 (2008).
  98. A. G. Shtukenberg, J. Freudenthal, and B. Kahr, "Reversible twisting during helical hippuric acid crystal growth," *J. Am. Chem. Soc.* **132**, 9341–9349 (2010).
  99. H.-M. Ye, J. Xu, F. J., and B. Kahr, "On the circular birefringence of polycrystalline polymers: polylactide," *J. Am. Chem. Soc.* **133**, 13848–13851 (2011).
  100. A. G. Shtukenberg, X. Cui, J. Freudenthal, E. Gunn, E. Camp, and B. Kahr, "Twisted crystalline mannitol needles establish homologous growth mechanisms for high polymer and small molecule ring-banded spherulites," *J. Am. Chem. Soc.* **134**, 6354–6364 (2012).
  101. X. Cui, A. L. Rohl, and K.-B. Shtukenberg, A., "Twisted aspirin crystals," *J. Am. Chem. Soc.* **135**, 3395–3398 (2013).
  102. A. G. Cui, X. and Shtukenberg, S. M. Nichols, and B. Kahr, "Circular birefringence in banded spherulites," *J. Am. Chem. Soc.* **136**, 5481–5490 (2013).
  103. X. Cui, S. M. Nichols, O. Arteaga, J. Freudenthal, F. Paula, A. G. Shtukenberg, and B. Kahr, "Dichroism in helicoidal crystals," *J. Am. Chem. Soc.* **138**, 12211–12218 (2016).